AIAA JOURNAL
Vol. 35, No. 2, February 1997

Computation of Acoustic Waves Through Sliding-Zone Interfaces

Christopher L. Rumsey*
NASA Langley Research Center, Hampton, Virginia 23681-0001

The effect of a patched sliding-zone interface on the transmission of acoustic waves is examined for two- and three-dimensional model problems. A simple but general interpolation scheme at the patched boundary passes acoustic waves without distortion, provided that a sufficiently small time step is taken. A guideline is provided for the maximum permissible time step or zone speed that gives an acceptable error introduced by the sliding-zone interface.

Introduction

THE prediction and control of ducted fan noise are important elements of aircraft engine design programs. Current methods of prediction rely extensively on field measurements and analytical scaling techniques. As computers continue to become more powerful, Euler and Navier–Stokes computer codes for ducted-fan noise prediction have become increasingly affordable. Recent advances in algorithms[1–3] that can enhance the efficiency of time-accurate Euler and Navier–Stokes computations also make difficult computations, such as three-dimensional rotor–stator interactions, better suited for inclusion in future engine design cycles.

Previous work by Rai[4] and Gundy-Burlet et al.[5] demonstrated the feasibility of using Navier–Stokes computations for time-accurate rotor–stator interactions. Gundy-Burlet et al. utilized a combination of overlapping and patched grids; the motion of the rotor relative to the stator was accomplished by "sliding" the rotor grid system past the stator grid system and using a nonconservative linear interpolation to transfer information between the two grid systems. Hall and Delaney[6] used a similar patched sliding-zone interface strategy to compute ducted prop-fan flows. Chen and Chakravarthy[7] utilized patched sliding-zone interfaces to perform rotor–stator computations. They used a simple piecewise-constant projection of flow variables between grid zones, with an area-weighting strategy. Janus and Whitfield[8] utilized localized grid distortion to pass information between zones that move relative to one another in a prop-fan simulation. Rather than employ interpolation, grid points near the zone interface were distorted and then "clicked" to new positions when appropriate. In Refs. 4–8, the focus of the computations was the prediction of global aerodynamic characteristics. Rangwalla and Rai[9] compared the numerically calculated tonal acoustics with theoretical values for a two-dimensional rotor–stator interaction. Emphasis was placed on the effects of boundary conditions and boundary extent; however, the effect of the patched sliding-zone interface on the accuracy of simulating the passage of acoustic waves was not explored.

Because accurate prediction of acoustic waves is essential to any noise-prediction analysis, the effect of the sliding-zone interface on the passage of such waves must be addressed. In the present paper, the effect of a patched sliding-zone interface similar to that employed in Refs. 5–7 is examined for several two-dimensional problems as well as for passage of a typical rotor–stator interaction mode through a three-dimensional duct with a rotating zone. The effects of time step and speed of the moving zone are examined; an engineering rule of thumb for maximum permissible time step or zone speed is developed.

Presented as Paper 96-1752 at the AIAA/CEAS 2nd Aeroacoustics Conference, State College, PA, May 6–8, 1996; received May 18, 1996; revision received Oct. 7, 1996; accepted for publication Oct. 14, 1996; also published in *AIAA Journal on Disc*, Volume 2, Number 2.

*Research Scientist, Fluid Mechanics and Acoustics Division, Mail Stop 128. Senior Member AIAA.

Description of the Code

The computer code CFL3D[10] solves the three-dimensional time-dependent thin-layer Navier–Stokes equations with an upwind finite-volume formulation. However, for the applications here, only the inviscid (Euler) equations are solved. This code can solve flows over multiple-zone grids that are connected in a one-to-one, patched, or overset manner and can employ grid sequencing, multigrid, and local time stepping in accelerating convergence to steady state. Upwind-biased spatial differencing is used for the inviscid terms, and flux limiting is used to obtain smooth solutions in the vicinity of shock waves. Viscous terms, when used, are centrally differenced. The equations are solved implicitly with the use of a three-factor approximate factorization (AF). Either the flux-difference-splitting (FDS) method of Roe[11] or the flux-vector-splitting method of Van Leer[12] can be used to obtain fluxes at the cell faces. The FDS approach is used for all results in this paper.

Time Advancement and Subiteration Algorithm

The CFL3D code is advanced in time with an implicit AF method. The implicit spatial derivatives are first-order accurate, which results in block-tridiagonal inversions for each sweep. However, for solutions that utilize FDS the block-tridiagonal inversions are further simplified with a diagonal algorithm; when the viscous terms are used, a spectral radius scaling is employed.

Second-order temporal accuracy for a single-step AF scheme is forfeited for unsteady computations with these simplifications to the left-hand side. One method for recovering the desired accuracy is through the use of subiterations. Two subiteration strategies have been implemented in CFL3D. These strategies were explored in detail by Rumsey et al.[3] The method employed for the computations in this paper is termed the pseudo time subiteration (or τ-TS) method, which uses a second-order-accurate temporal discretization. In the literature (e.g., Ref. 13), the τ-TS method is also referred to as the dual time method because a pseudo time is used to iterate to the next desired physical time. The chief advantage to the τ-TS subiteration strategy is that it frees the user from numerical constraints on the time step; an appropriate physical time step can be selected to resolve the physics of the flow in question.

Dynamic Patched-Grid Algorithm

A patched-grid interface implies that two zones share a common interface at which the grid points do not necessarily connect in a one-to-one manner. For grids in relative motion to one another (for example, when a grid zone around a rotor slides past a grid zone around a stator), dynamic patched interfacing is a relatively easy way to handle the transfer of time-accurate data between zones.

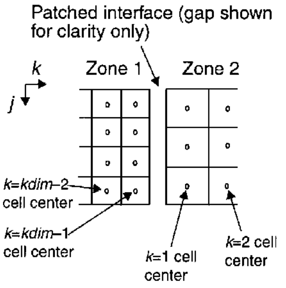

Fig. 1 Sample two-dimensional patched interface.

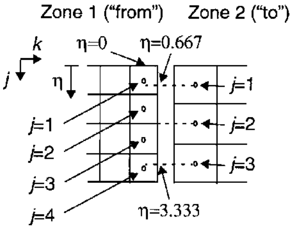

Fig. 2 Sample two-dimensional patched interface, with zone 2 as "to" zone.

In CFL3D, the patching is accomplished nonconservatively in the following way. First, at the patched interface, the problem is reduced by one degree of freedom because data are used only in the two planes of cell centers in computational space nearest each interface to update the ghost-cell boundary conditions in the other zone. For example (as shown in Fig. 1 in two dimensions), if the $k = kdim$ boundary of zone 1 interfaces with the $k = 1$ boundary of zone 2, then zone 2 obtains information for its two ghost cells from the $k = kdim - 1$ and $k = kdim - 2$ cell centers of zone 1; zone 1 obtains information for its two ghost cells from the $k = 1$ and $k = 2$ cell centers of zone 2.

Interpolation is accomplished dynamically at each time step (every time the moving zone changes position). For each face center point on the interface in the "to" zone, a corresponding real-valued index location is determined in the "from" zone. The primitive variables are then interpolated to this real-valued index location. A simple two-dimensional example is given in Fig. 2; zone 2 acts as the "to" zone, and only one row of ghost cells is shown in the "from" zone for clarity. In this example, the center point of the cell $j = 1$ in zone 2 lines up with $\eta = 0.6667$ in zone 1, which lies in the cell $j = 1$ of zone 1. Therefore, this particular ghost-cell boundary condition is interpolated by using the primitive variables at $j = 1$ in zone 1 and an appropriately weighted fraction of the η-direction gradient at $j = 1$. Further details of the patched-grid algorithm are given in Biedron and Thomas.[14]

When periodic boundary conditions are applied and one grid zone slides relative to another, copies of both the moving and nonmoving zones must be supplied, which are translated or rotated appropriately to ensure that each "to" zone has a "from" neighbor at all times and vice versa. To avoid the necessity of making too many copies over long times, the current algorithm also periodically rotates or translates the moving block and its solution whenever its movement exceeds a specified limit.

Results

Several two- and three-dimensional model problems are examined to study the effect of a patched sliding-zone interface on the passage of acoustic waves. Unless otherwise noted, three τ-TS subiterations with three levels of multigrid are used for the results in this paper.

Two-Dimensional Axially Moving Acoustic Waves

The first test case involves acoustic waves that are moving axially in two dimensions (x, z). At the left end of a computational domain, waves are generated by perturbing the freestream pressure levels in accordance with

$$p = p_0 + h\cos\left(\frac{2\pi t}{T_t}\right)\cos\left(\frac{2\pi z}{T_z}\right) \tag{1}$$

where p_0 is the nondimensional freestream static pressure ($=1/\gamma$) and h is taken as 0.04518. Time is nondimensionalized by unit length and speed of sound. The freestream is quiescent.

This test case is patterned after a computation by Khan,[15] who used a perturbational form of the Euler equations to compute the nonlinear behavior of a plane acoustic wave that was propagating axially; the results were compared with the theoretical predictions of Pierce[16] at locations prior to where nonlinear steepening causes shock formation. In the current study, a sinusoidal transverse variation of pressure (in the z direction) is also imposed to test the effect of a sliding-zone interface (no effect is realized otherwise). Comparison with the theoretical results is made at a transverse location at which the acoustic wave front is aligned with the z axis. The variation in the z direction is gradual enough to allow the wave to approximate a plane wave at this location.

The computation is performed by using either one or two zones. In the latter case, zone 2 slides in the z direction along one end of zone 1; a patched sliding-zone interface connects the two zones (see Fig. 3). The upper and lower boundaries are treated as periodic interfaces, and the right boundary employs a characteristic boundary condition. To minimize the possibility of spurious reflections from the right boundary, the grid is stretched in the x direction past $x = 1.6345$.

The parameter T_t is taken as 0.55164 (which corresponds to a frequency of 0.6 kHz in air), and T_z is taken as 3.2. This latter parameter yields one complete period of pressure fluctuation between $z = 0$ and $z = 3.2$.

Before evaluating the effect of the sliding-zone interface, parametric studies were used to determine the grid size and time step necessary to capture the physics of this flowfield with the CFL3D code. Figure 4 shows the effect of varying the number of cells in the z direction from 8 to 64. The rms error in the pressure between successive grid solutions decreases from 0.0033 to 0.00081 to 0.00019. These errors vary quadratically with mesh size, as expected for a second-order spatially accurate scheme. The rms error from an infinitely fine grid solution can be extrapolated to be approximately 4.3×10^{-3}, 1.1×10^{-3}, 2.6×10^{-4}, and 6.5×10^{-5} for 8, 16, 32, and 64 points, respectively. Therefore, 32 grid points yield less than 0.6% rms error, normalized by the magnitude of the pressure perturbation h, and are considered sufficient to depict the sinusoidal variation in the acoustic pressure.

The effect of Δx is shown in Figs. 5 and 6. The wavelength in the x direction for this case is 0.552. Using a constant Δz spacing of 0.1 (32 points per wave in the z direction), the Δx spacing is varied from 0.02554 (approximately 22 points per wave) to 0.006385 (approximately 86 points per wave). Figure 5 shows the pressure as

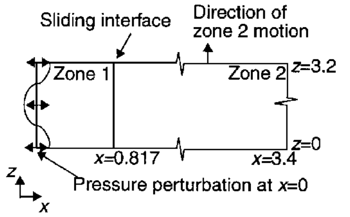

Fig. 3 Sketch of two-dimensional case for axially moving acoustic waves.

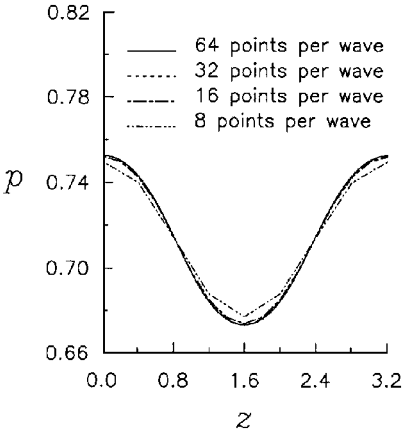

Fig. 4 Effect of number of points in z direction on pressures at $x = 0.83$, with $\Delta x = 0.01277$, $\Delta t = 0.005$, and $T = 3.6$.

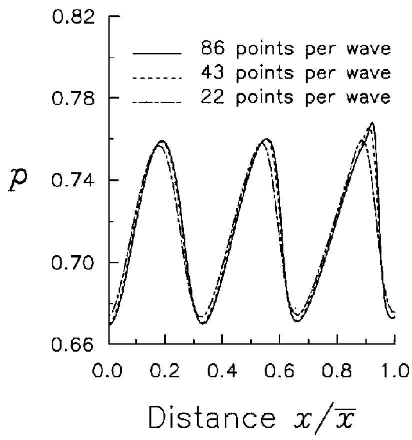

Fig. 5 Effect of number of points in x direction on pressures at $z = 0$, with $\Delta z = 0.1$, $\Delta t = 0.005$, and $T = 3.6$.

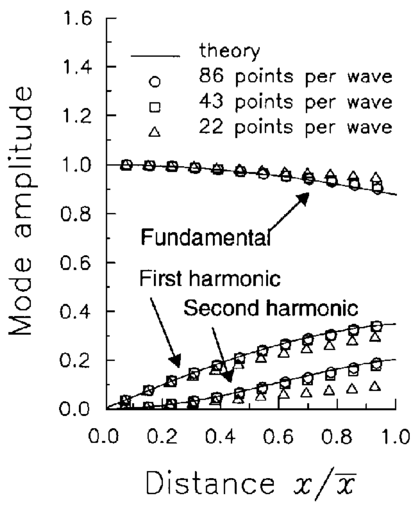

Fig. 6 Effect of number of points in x direction on harmonics at $z = 0$, with $\Delta z = 0.1$ and $\Delta t = 0.005$.

a function of $x/\bar{x}$ along $z = 0$, where $\bar{x}$ is the value of the distance at which the shock forms:

$$\bar{x}' = \left(\frac{2}{\gamma + 1}\right)\frac{\rho' a'^2}{k' h'} \tag{2}$$

($'$ indicates a dimensional quantity). In this equation, $k' = \omega'/a'$, ω' is the frequency in radians per second, ρ' is the density, and a' is the speed of sound. For this case, $\bar{x} = 1.6194$. Figure 6 shows the amplitude of the fundamental and the first two harmonics as a function of distance. The computational curves in this figure are generated by establishing a periodic solution, computing over a nondimensional time of 1.1, and using a Fourier decomposition on the time histories of pressure at each spatial location. Three higher harmonics are computed; for clarity, only the first two are shown in Fig. 6. The predicted fundamental and the first two harmonics agree well with the theoretical predictions of Pierce[16]; with 43 points per wave, the maximum error (nearest $x/\bar{x} = 1$) is $+2.2\%$, -1.0%, and -7.9% for the fundamental and first two harmonics, respectively. With only 22 points per wave, significant error is realized as $x/\bar{x}$ approaches 1: the first harmonic is underpredicted by 14% and the second harmonic is underpredicted by 52%.

The effect of time step is shown in Fig. 7. A time step of $\Delta t = 0.01$ (55 steps per cycle) is sufficient to capture the fundamental and first harmonic but is not sufficient for the higher harmonics. A time step of $\Delta t = 0.005$ (110 steps per cycle) is temporally converged on this grid for all harmonics up to the third harmonic; further refinement in time step makes less than a 1% change in the fundamental and first two harmonics and less than a 5% change in the third harmonic.

In summary, the nondimensional grid size necessary for the current numerical algorithm to accurately capture the physics of this

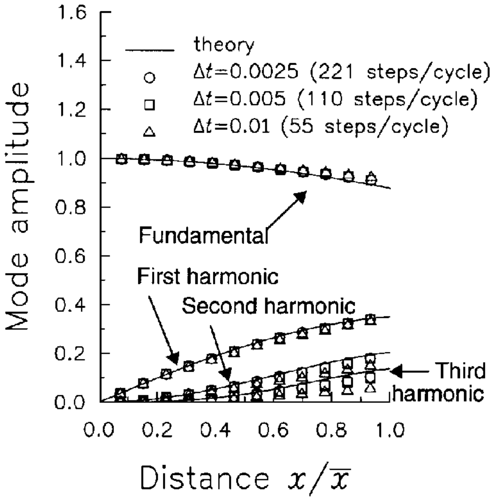

Fig. 7 Effect of time step on harmonics at $z = 0$, with $\Delta x = 0.01277$ and $\Delta z = 0.1$.

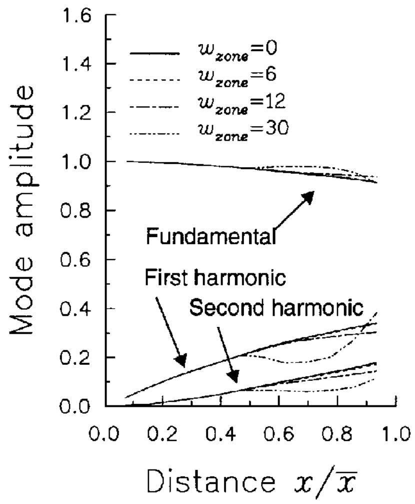

Fig. 8 Effect of zone speed on harmonics at $z = 0$, with $\Delta x = 0.01277$, $\Delta z = 0.1$, and $\Delta t = 0.005$.

flow to within the level of accuracy described above is as follows: $\Delta z = 0.1$ (32 points per transverse wave) and $\Delta x = 0.01277$ (43 points per axial wave). The nondimensional time step necessary is $\Delta t = 0.005$ (110 steps per cycle). This baseline grid and time step are utilized to assess the effect of a sliding-zone interface.

Although not shown, a two-zone grid with zone 2 held stationary yields a solution that is identical to the single-zone solution. When zone 2 slides past zone 1 at a constant velocity, the solution becomes distorted as the zone speed increases, as shown in Fig. 8. In this plot, the theoretical predictions and the third harmonic are not shown, and, for clarity, the computed results are displayed as lines rather than symbols. The zonal interface is at $x/\bar{x} = 0.5047$. Up to a speed of roughly $w_{\text{zone}} = 6$ (nondimensionalized by the speed of sound; i.e., $M_{\text{zone}} = 6$), the solution is essentially unaffected (the change in predicted harmonic mode amplitudes is less than 4%). At $w_{\text{zone}} \geq 12$, however, the solution deteriorates significantly.

At a time step of $\Delta t = 0.005$ and a zone speed of $w_{\text{zone}} = 6$, zone 2 slides past one periodic variation in the acoustic data (i.e., the space over which the flowfield is periodic in the z direction) in approximately 107 time steps. This parameter can be used as a rule-of-thumb indicator of the limit on the time step when a sliding zone is present. Extensive investigation by the author (not all of which is reported here) indicates that if a zone is sliding past another zone and flowfield spatial variations in the direction of zone motion are present, then the time step must be set to allow approximately 80 or more time steps for the moving zone to traverse one period of

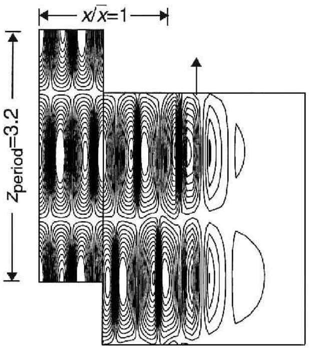

Fig. 9 Pressure contours with $\Delta t = 0.001$, $T = 3.6$, and $w_{\text{zone}} = 30$.

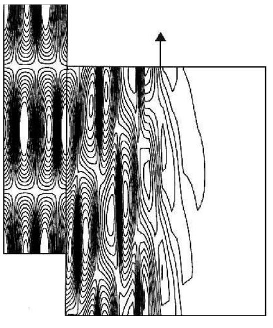

Fig. 10 Pressure contours with $\Delta t = 0.005$, $T = 3.6$, and $w_{\text{zone}} = 30$.

that variation. This rule of thumb is summarized by the following equations:

$$\left|(w_{\text{zone}})_{\max} - w_{\text{data}}\right| \approx \frac{z_{\text{period}}}{80\Delta t} \tag{3}$$

or

$$\Delta t_{\max} \approx \frac{z_{\text{period}}}{80\left|w_{\text{zone}} - w_{\text{data}}\right|} \tag{4}$$

where z_{period} is the spatial distance in the direction of zone motion over which the flowfield varies by approximately one period and w_{data} is the component of the acoustic-wave velocity parallel to the moving-zone interface. Because this rule of thumb is based only on qualitative estimates of acceptable error, it is best used as a guideline for establishing an initial estimate for the maximum time step or zone speed. Further refinement to the desired tolerance can be made through parametric studies.

In the case of axially moving waves, $w_{\text{data}} = 0$. If the time step is fixed at $\Delta t = 0.005$, then the maximum zone speed according to the guideline is roughly 8. This conclusion is consistent with the results in Fig. 8. If, on the other hand, the zone speed is fixed at $w_{\text{zone}} = 30$, then the time step must be no larger than $\Delta t \approx 0.0013$. The results obtained with $\Delta t = 0.001$ and $w_{\text{zone}} = 30$ are contrasted with those obtained with $\Delta t = 0.005$ and $w_{\text{zone}} = 30$ in Figs. 9 and 10. The former result shows little distortion of the pressure contours in zone 2, whereas the latter shows large distortion. The oval contours should travel left to right only, with some compression, and then diminish past $x/\bar{x} = 1$, where the grid is stretched.

This rule of thumb is independent of grid spacing in the direction of zone motion. Although not shown, two-zone results with 17, 33, and 65 grid points in the z direction yield nearly identical results when Δt and w_{zone} are held fixed. Also, if zone 1 is clustered so that Δz varies from 0.1 to 0.0001 while zone 2 retains uniform grid spacing, the results again follow the same rule of thumb. The number of τ-TS multigrid subiterations currently used (3) is sufficient to drive the L_2 norm of the equation for density down by at least 1.5 orders of magnitude for each time step. The use of six subiterations drives the residual down 3.5 orders for each time step, with no perceptible change in the solution.

Two-Dimensional Vibrating Plates

The following two-dimensional model problem is patterned after a computation by Huff.[17] An infinite row of vibrating flat plates is simulated on the rectangular domain depicted in Fig. 11. The plates, of chord length c', are separated by height $h = h'/c' = 1$.

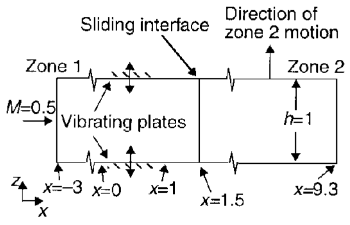

Fig. 11 Sketch of two-dimensional vibrating-plate case.

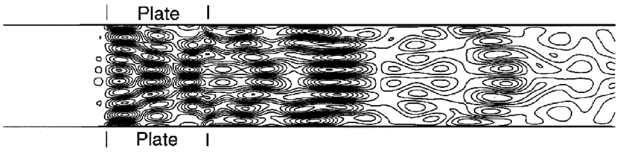

Fig. 12 Pressure contours with one zone, $\Delta t = 0.00125$ and $T = 5$.

Slip-velocity (Euler) boundary conditions are applied on the plates, and periodic boundary conditions are applied elsewhere on the upper and lower boundaries. The left and right boundaries employ a characteristic boundary condition, and the grid is stretched in the x direction past $x = x'/c' = 5$. When used, a sliding-zone interface is employed at a location 0.5 chord length downstream of the trailing edge of the plates, which vibrate in phase with each other in accordance with

$$z' = h' \sin(\omega' t') \tag{5}$$

where ω' is the frequency in radians per second.

If the lengths are nondimensionalized by c' and time by c'/a'_∞ and the reduced frequency is defined as

$$k = \frac{\omega'(c'/2)}{u'_\infty} \tag{6}$$

then the nondimensional equation that defines the plate vibration becomes

$$z = h \sin(M_\infty k t/2) \tag{7}$$

Here, h is taken as 0.00004, $k = 8\pi$, and $M_\infty = 0.5$. Many acoustic waves generated by this test problem travel at an oblique angle in both directions relative to the sliding interface. At this frequency, approximately four complete cycles of pressure variation span the space between the plates. Hence, $z_{\text{period}} \approx 0.25$. A vertical uniform grid spacing of $\Delta z = 0.0078125$ is used, which results in a spatial resolution of approximately 32 grid points per wave. The grid spacing in the axial direction is $\Delta x = 0.03125$ between $x = -3$ and $x = 5$ and is stretched past $x = 5$. Although not shown, parametric studies indicate that this grid spacing is adequate to spatially resolve this flowfield.

Because this model problem is based loosely on the types of acoustic waves that may be generated by vibrating stator vanes in an engine, computations are carried out with a fixed zone speed that is comparable to that of a typical maximum rotor tip speed. Hence, $w_{\text{zone}} = 1.2$ is chosen; this value corresponds to a tip Mach number of $M = 1.2$. Equation (4), with $w_{\text{data}} = \pm 1$ (because the waves travel obliquely to the zone interface with a maximum speed equal to the speed of sound), is used to determine a maximum time step of $\Delta t_{\max} \approx 0.0014$. Time-step studies (not shown) indicate that the time step necessary to adequately resolve the physics of this flowfield is approximately $\Delta t = 0.0025$, which corresponds to 400 time steps per period of plate oscillation. Hence, given the fixed zone speed of $w_{\text{zone}} = 1.2$ in this case, the time-step constraint that is attributable to zone motion is more restrictive than the time-step constraint needed to adequately resolve the flowfield.

Because of the limitation caused by zone motion, the time step $\Delta t = 0.00125$ is used. Pressure contours (nondimensionalized by $\rho'_\infty a'^2_\infty$) for a single zone are shown in Fig. 12. Contour levels range from 0.712 to 0.716 in steps of 0.0002. Figure 13 shows contours of pressure differences between the single-zone solution and two-zone solutions (with the second zone sliding). Results using two time steps, $\Delta t = 0.00125$ and $\Delta t = 0.0025$, are shown. Contour levels

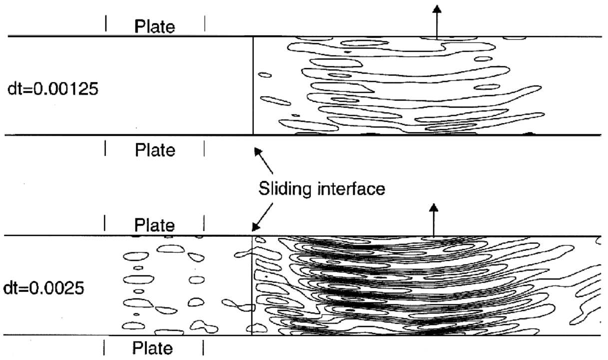

Fig. 13 Contours of pressure differences between two-zone and single-zone computations with T = 5 and w_{zone} = 1.2.

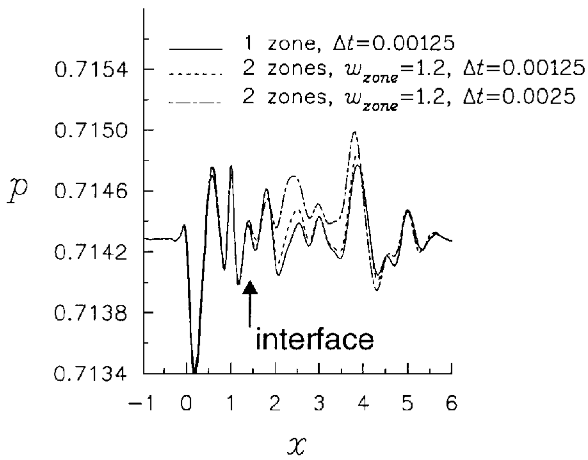

Fig. 14 Pressures along z = 0.75 with T = 5.

range from −0.0007 to 0.0007 in steps of 0.00015. Results with the smaller time step are only slightly affected by the sliding-zone interface (maximum error is 0.00025 and rms error is 4.7×10^{-5}), whereas results with the larger time step show greater distortion of the acoustic waves both before and after they have passed through the zone interface (maximum error is 0.00068 and rms error is 1.6×10^{-4}). Additional details of these differences are shown in Fig. 14, which is a plot of pressure levels as a function of x along a line at $z = 0.75$.

Three-Dimensional Rotor–Stator Interaction Mode

To assess the passage of acoustic waves through a sliding-zone interface in a more realistic configuration, theoretical rotor–stator interaction modes are derived based on a 16-blade 20-vane model,[18] with duct radius $r' = 0.1393$ m, Mach number $M = 0.6$, and rotor speed is 16,900 rpm. The theoretical levels of pressure perturbation are

$$p'(r', \theta, x') = A' J_m(k'_r r') \exp i[a' k' t' - m\theta - k'_a x'] \qquad (8)$$

where A' is the magnitude of the perturbation, taken as 0.001 p'_0 (p'_0 is taken as 100,000 Pa), and J_m is the Bessel function of order m. One of the propagating modes [for a single blade passage frequency (BPF)] is the (−4, 1) mode, where $m = -4$ is the circumferential mode number and $n = 1$ is the radial mode number. For a single BPF, $k' = 87.97\ \mathrm{m}^{-1}$; for the (−4, 1) mode, $k'_r = 38.17\ \mathrm{m}^{-1}$ and $k'_a = -211.37\ \mathrm{m}^{-1}$. This mode spins in the direction opposite that of the rotor. Other propagating modes are investigated in Rumsey.[19]

To test whether the (−4, 1) acoustic mode can be propagated undistorted through a patched sliding-zone interface, a three-dimensional time-accurate computation is performed in a cylindrical duct. Because the (−4, 1) mode is periodic over $\pi/2$, the grid used is a quarter of a cylinder. The grid extends from $x' = -0.5$ to $x' = 0$ m and is divided into three zones. The middle zone, which extends from $x' = -0.2786$ to $x' = -0.1393$ m, can be rotated. Time-dependent pressure perturbations are imposed at the downstream boundary (at $x' = 0$) with Eq. (8).

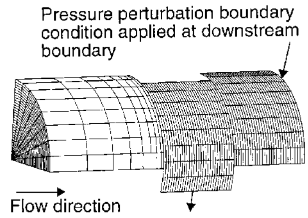

Fig. 15 A 273 × 33 × 33 duct grid (points removed for clarity).

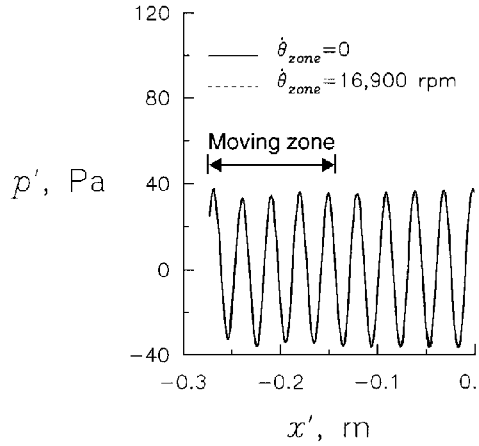

Fig. 16 Pressures along duct wall with Δt = 0.001 and T = 0.8.

On the basis of grid studies (not shown), the grid that represents the best compromise between accuracy and efficiency for this case is 273 × 33 × 33, with $\Delta x' = 0.00116$ m in the unstretched portion of the mesh. This grid size yields 33 points per wave in the circumferential direction and approximately 25 points per wave in the axial direction, which is sufficient to propagate this mode through both downstream zones with reasonably minimal phase shift and attenuation. (Maximum pressure levels are computed to be approximately ±35 Pa, whereas the exact linear solution is ±40 Pa.) The radial and circumferential spacing is uniform, and the axial spacing is uniform in the two downstream zones (with 121 grid points each) and is stretched in the upstream zone. The grid, with every fourth grid point plotted in the axial and circumferential directions for clarity, is shown in Fig. 15. The middle zone is shown in a rotated position.

Time-step studies (also not shown) indicate that at least 36–71 time steps per period are required to propagate this mode through both downstream zones with minimal attenuation and phase shift. Therefore, a nondimensional time step $\Delta t = 0.001$ is employed, which corresponds to 71 time steps per period for BPF.

The three-dimensional duct acoustic modes show less sensitivity to a moving zone than the two-dimensional test cases. A minimum of approximately 40 (rather than 80) time steps is required for the moving zone to pass one spatially periodic variation in the flowfield. Therefore, for rotating zones, Eqs. (3) and (4) are modified to read as

$$\left|(\dot{\theta}_{zone})_{max} - \dot{\theta}_{data}\right| \approx \frac{\theta_{period}}{40\Delta t} \qquad (9)$$

or

$$\Delta t_{max} \approx \frac{\theta_{period}}{40\left|\dot{\theta}_{zone} - \dot{\theta}_{data}\right|} \qquad (10)$$

A fixed moving-zone speed of $\dot{\theta}_{zone} = 16{,}900$ rpm results in a maximum allowable nondimensional time step of $\Delta t_{max} \approx 0.0014$ (with $\theta_{period} = 90$ deg and $\dot{\theta}_{data} = -67{,}600$ rpm). This time-step limitation that results from zone motion is slightly higher than the time step of $\Delta t = 0.001$ necessary to resolve the physics of the flow (regardless of zone motion). Therefore, for this case, the constraint due to the numerical resolution of the physics is more restrictive than the constraint due to zone motion, and the zone motion is expected to have little or no discernible effect on the temporally resolved solution.

The acoustic waves generated by the downstream perturbation propagate upstream in a spiral manner. A total nondimensional time of $T = 0.8$ is sufficient to achieve a periodic solution through the two downstream zones. Figure 16 shows pressure perturbation levels

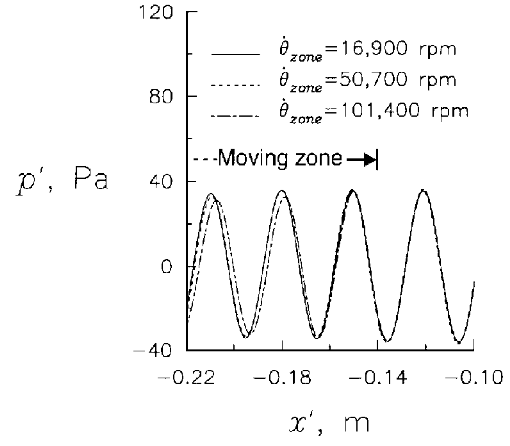

Fig. 17 Effect of zone speed on pressures along duct wall with Δt = 0.001 and T = 0.8.

as a function of x' along the duct wall at a $\theta =$ constant location for a nonrotating zone and for a zone that is rotating at 16,900 rpm. Results are essentially identical for both cases, which indicates, as expected, that the sliding-zone interface does not distort the $(-4, 1)$ mode acoustic waves with this grid and time step. Each computation requires approximately 4 h of CPU time on a Cray Y-MP computer.

Figure 17 shows the effect of increasing the zone rotation speed. Tripling the rotation speed results in negligible distortion, whereas quintupling the speed changes the character of the solution upstream of the moving-zone interface. With Eq. (9), a time step of $\Delta t = 0.001$ allows for a maximum zone speed of 53,113 rpm. This maximum speed is consistent with the results in the figure. Five subiterations are required for the higher zone speeds.

Conclusions

Patched sliding-zone interfaces, in combination with the time-accurate Euler and Navier–Stokes equations, are often employed for aerodynamic computations of rotor–stator interactions. However, before codes with sliding interfaces can be used as a major part of any noise-prediction effort, the accuracy with which acoustic waves are passed through the sliding-zone interfaces must be assessed. Preliminary findings indicate that an important factor that contributes to the accuracy of acoustic-wave passage is the number of time steps required for the sliding zone to move past spatial variations in the flowfield that exist in the direction parallel to the sliding-zone interface (e.g., circumferential variations for duct flows). To avoid unreasonable distortions, at least 40–80 time steps are required for the sliding zone to pass one period of the spatial variation. If the time step is too large, then distortions in the acoustic waves result. This rule of thumb has been demonstrated for two simple two-dimensional test problems as well as for a three-dimensional-duct test problem.

Acknowledgments

The author acknowledges R. Biedron of AS&M, Inc., Hampton, Virginia, for coding the dynamic patched interface routines and for general CFL3D code support as well as for helpful discussions throughout the investigation. The author also thanks the other members of the Langley Ducted Fan Noise Prediction Team for their assistance: leader F. Farassat, C. Hsu, P. Spence, and M. Dunn. Thanks are also due to M. Janus at Mississippi State University for many helpful discussions and to D. Huff at NASA Lewis Research Center for sparking the initial interest in this study.

References

[1]Jameson, A., "Time Dependent Calculations Using Multigrid, with Applications to Unsteady Flows Past Airfoils and Wings," AIAA Paper 91-1596, June 1991.

[2]Melson, D., Sanetrik, M., and Atkins, H., "Time-Accurate Navier–Stokes Calculations with Multigrid Acceleration," *Sixth Copper Mountain Conference on Multigrid Methods*, NASA CP-3224, Pt. 2, Nov. 1993, pp. 423–437; also *Proceedings of the AIAA 11th Computational Fluid Dynamics Conference*, (Orlando, FL), Pt. 2, AIAA, Washington, DC, 1993, pp. 1041, 1042.

[3]Rumsey, C., Sanetrik, M., Biedron, R., Melson, N., and Parlette, E., "Efficiency and Accuracy of Time-Accurate Turbulent Navier–Stokes Computations," *Computers and Fluids*, Vol. 25, No. 2, 1996, pp. 217–236.

[4]Rai, M., "Three-Dimensional Navier–Stokes Simulations of Turbine Rotor-Stator Interaction, Parts I and II," *Journal of Propulsion and Power*, Vol. 5, No. 3, 1989, pp. 307–319.

[5]Gundy-Burlet, K., Rai, M., and Dring, R., "Two-Dimensional Computations of Multi-Stage Compressor Flows Using a Zonal Approach," AIAA Paper 89-2452, July 1989.

[6]Hall, E., and Delaney, R., "Investigation of Advanced Counterrotation Blade Configuration Concepts for High Speed Turboprop Systems," NASA CR 187126, Jan. 1993.

[7]Chen, C., and Chakravarthy, S., "Calculation of Unsteady Rotor/Stator Interaction," AIAA Paper 90-1544, June 1990.

[8]Janus, M., and Whitfield, D., "Counterrotating Prop-Fan Simulations Which Feature a Relative-Motion Multiblock Grid Decomposition Enabling Arbitrary Time Steps," AIAA Paper 90-0687, Jan. 1990.

[9]Rangwalla, A., and Rai, M., "A Numerical Analysis of Tonal Acoustics in Rotor-Stator Interactions," *Journal of Fluids and Structures*, Vol. 7, No. 6, 1993, pp. 611–637.

[10]Thomas, J., Krist, S., and Anderson, W., "Navier–Stokes Computations of Vortical Flows over High Aspect-Ratio Wings," *AIAA Journal*, Vol. 28, No. 2, 1990, pp. 205–212.

[11]Roe, P., "Approximate Riemann Solvers, Parameter Vectors, and Difference Schemes," *Journal of Computational Physics*, Vol. 43, No. 2, 1981, pp. 357–372.

[12]Van Leer, B., "Flux Vector Splitting for the Euler Equations," *Lecture Notes in Physics*, Vol. 170, 1982, pp. 501–512.

[13]Venkateswaran, S., and Merkle, C., "Dual Time Stepping and Preconditioning for Unsteady Computations," AIAA Paper 95-0078, Jan. 1995.

[14]Biedron, R., and Thomas, J., "A Generalized Patched-Grid Algorithm with Application to the F-18 Forebody with Actuated Control Strake," *Computing Systems in Engineering*, Computational Technology for Flight Vehicles, Vol. 1, Nos. 2–4, edited by A. Noor and S. Venneri, Pergamon, Oxford, England, UK, 1990, pp. 563–576.

[15]Khan, M., "Computations of Aeroacoustic Fields Using Finite Volume Method," *Computational Acoustics: Algorithms and Methods*, edited by D. Lee, R. L. Sternberg, and M. H. Schultz, Elsevier, Amsterdam, 1988, pp. 83–101.

[16]Pierce, A., *Acoustics, An Introduction to Its Physical Principles and Applications*, Acoustical Society of America, American Inst. of Physics, New York, 1989, pp. 571–573.

[17]Huff, D., "Pressure Wave Propagation Studies for Oscillating Cascades," AIAA Paper 92-0145, Jan. 1992; also NASA TM-105406, Jan. 1992.

[18]Thomas, R., Gerhold, C., Farassat, F., Santa Maria, O., Nuckolls, W., and DeVilbiss, D., "Far Field Noise of the 12 Inch Advanced Ducted Propeller Simulator," AIAA Paper 95-0722, Jan. 1995.

[19]Rumsey, C., "Computation of Acoustic Waves Through Sliding-Zone Interfaces Using an Euler–Navier–Stokes Code," AIAA Paper 96-1752, May 1996.